Applied Physics Letters

Ultrabroadband and independent polarization of optical amplification with InGaAs-based indium-rich cluster quantum-confined structure

Cite as: Appl. Phys. Lett. **116**, 252106 (2020); https://doi.org/10.1063/5.0008799
Submitted: 25 March 2020 . Accepted: 12 June 2020 . Published Online: 24 June 2020

Ming Zheng, Qingnan Yu, Xue Li, Hanxu Tai, Xing Zhang, Jianwei Zhang, Yongqiang Ning, and Jian Wu

Applied Physics Letters ARTICLE scitation.org/journal/apl

Ultrabroadband and independent polarization of optical amplification with InGaAs-based indium-rich cluster quantum-confined structure

Cite as: Appl. Phys. Lett. **116**, 252106 (2020); doi: 10.1063/5.0008799
Submitted: 25 March 2020 · Accepted: 12 June 2020 ·
Published Online: 24 June 2020

Ming Zheng,[1] Qingnan Yu,[2,a)] Xue Li,[3] Hanxu Tai,[1] Xing Zhang,[3] Jianwei Zhang,[3] Yongqiang Ning,[3] and Jian Wu[1,a)]

AFFILIATIONS

[1]School of Physics, Beihang University, Beijing 100191, China
[2]College of Physics and Telecommunication Engineering, Zhoukou Normal University, Zhoukou 466001, China
[3]State Key Laboratory of Luminescence and Application, Changchun Institute of Optics, Fine Mechanics and Physics, Chinese Academy of Sciences, Changchun 130033, China

[a)]**Authors to whom correspondence should be addressed:** yuqingnan666@163.com and jwu2@buaa.edu.cn

ABSTRACT

This Letter reports polarization-independent optical amplification over an ultrabroad spectral range by semiconductor optical amplifiers. The technique uses an InGaAs-based indium-rich cluster (IRC) quantum-confined structure as the active medium and obtains comparable optical gain for both transverse electric (TE) and transverse magnetic (TM) polarization modes in the spectral ranges of 905–1005 and 905–970 nm, respectively. The device thus provides independent optical amplification for TE and TM polarizations over a common bandwidth of 65 nm. The difference between the amplified intensities of TE and TM modes is <0.5 dB. These results are attributed to the special emission mechanism of the IRC quantum-confined structure, which differs from that of conventional quantum wells or quantum dots. A preliminary analysis of this mechanism is provided.

Semiconductor optical amplifiers (SOAs) play important roles in numerous applications, such as optical communication, optical signal processing, and pumping for high-power fiber lasers.[1–5] However, the narrow gain bandwidth and the polarization dependence of conventional quantum well or quantum dot SOAs restrict the application of SOAs. The narrow gain bandwidth is an inherent feature of conventional quantum wells and quantum dots, and the polarization dependence is generally due to the large gain difference between transverse electric (TE) and transverse magnetic (TM) polarization modes generated in strained quantum well and quantum dot devices. These features prevent SOA devices from being used for polarization-independent optical amplification of TE and TM modes.

Several methods have been proposed to overcome these problems and develop polarization-independent optical amplification over a broad spectral range from a quantum-confined device. For example, to obtain comparable TE and TM gain from quantum-well devices, some groups have constructed alternate active layers with compressive- and tensile-strained wells in a singlechip.[6–9] Others have combined compressively strained wells with tensile-strained barriers[10–12] or with a tensile-strained quaternary active layer.[13] In addition to developing various quantum-well structures for SOAs, quantum-dot SOA devices have been investigated. For these devices, columnar quantum dots surrounded by strained side barriers were developed, which led to polarization-independent TE and TM gain in the 1.5 μm band.[14,15] Although these efforts led to polarization-independent optical amplification from quantum-well and quantum-dot structures, the amplification bandwidth remains very limited.

Recently, we investigated the indium-rich cluster (IRC) effect in InGaAs/GaAs materials and found that it led to a different quantum confinement structure, which produced very interesting emission characteristics. For example, multiple peaks appeared in the gain spectrum from these devices, which allowed for dual-wavelengths lasing. This phenomenon is attributed to a modification of the carrier recombination competition that occurs in a conventional quantum well. The phenomenon is associated with the formation of IRCs that lead to multiple InGaAs regions with varying indium content within the gain medium.[16] Furthermore, comparable TE and TM gain from a single IRC quantum-confined device is possible, which means that polarization-independent optical amplification may be possible.

This Letter reports the use of an InGaAs-based IRC quantum-confined structure as gain medium to realize polarization-independent optical amplification over a broad spectral range. Unlike dual-wavelength lasing, the mechanism for achieving this goal is associated with hybrid strain and special energy bands that form within the material due to IRCs.

The approach replaces conventional quantum wells or quantum dots with an InGaAs-based IRC quantum-confined structure as gain medium. Because IRCs generally occur in highly strained InGaAs/GaAs systems, the active layer uses $In_{0.17}Ga_{0.83}As/GaAs/GaAsP_{0.08}$, in which the InGaAs layer is 10 nm thick. Investigations of IRCs have shown that the indium atoms migrate along the InGaAs growth direction to relax the high strain caused by the large lattice mismatch within the InGaAs/GaAs material. When more than a few monolayers of InGaAs are deposited on the GaAs, this process leads to a high concentration of island-like accumulations of indium atoms or InAs clusters on the surface of the InGaAs layer.[17–19] In the $In_{0.17}Ga_{0.83}As/GaAs/GaAsP_{0.08}$ system, the 2-nm-thick GaAs layer embedded between the $In_{0.17}Ga_{0.83}As$ layer and the 8-nm-thick $GaAsP_{0.08}$ barrier serves to reduce the strain.

This structure was grown with a V/III ratio of 40. The sample was deposited at 0.75 μm/h under a pressure of 100 mbar and a temperature of 660 °C. The high temperature increases the migration length of the indium atoms to allow for the formation of IRCs.[20] Figure 1(a) shows the sample composition, which is similar to the structure described in Ref. 16 and ensures the formation of IRCs. The epitaxial sample structure was grown by using metal-organic chemical vapor deposition on a GaAs (001) substrate.

Figure 1(b) shows an image of the clusters obtained by using atomic force microscopy (AFM) (Park Systems Instrument Co., Ltd., model XE100). Given that the design and growth of the sample satisfy the conditions for forming IRCs, the clusters imaged by AFM are identified as IRCs. Based on the AFM images, the cluster size ranges from 20 to 200 nm in width and from 2 to 8 nm in height.

During the growth of the material, the indium atom migration reduces the indium content in the $In_{0.17}Ga_{0.83}As$ regions, so the original active layer of $In_{0.17}Ga_{0.83}As$ material develops numerous smaller $In_xGa_{1-x}As$ regions of varying size and indium content ($x \leq 0.17$). The differing indium content and lattice mismatch in these $In_xGa_{1-x}As$ regions produce anisotropic strain, which is the mechanism by which comparable TE and TM gain is obtained over a broad spectral range for polarization-independent optical amplification.

To measure TE and TM gain, the sample was processed to obtain a 0.5 mm × 0.5 mm edge-emitting configuration. One end was coated to give a transmittance of $T = 99.99\%$ and the other end was left uncoated. Optical injection was achieved by irradiating the top surface of the SOA with a 20-ms-pulsed 808 nm laser, and the amplified photoluminescence (APL) spectrum from each end of the sample was recorded [see Fig. 2(a)]. The optically injected carrier density was 4.8×10^{17} cm^{-3} at a pump power of 16.5 W. The carrier density was calculated from the pump power by using[21]

$$N = \frac{\eta_{abs} P_p}{h\nu N_w L_w A_p} \tau(N), \quad (1)$$

where η_{abs} is the absorption efficiency of the pump, $h\nu$ is the pump photon energy, P_p is the pump power, and τ is the carrier lifetime, which is related to the monomolecular, bimolecular, and Auger

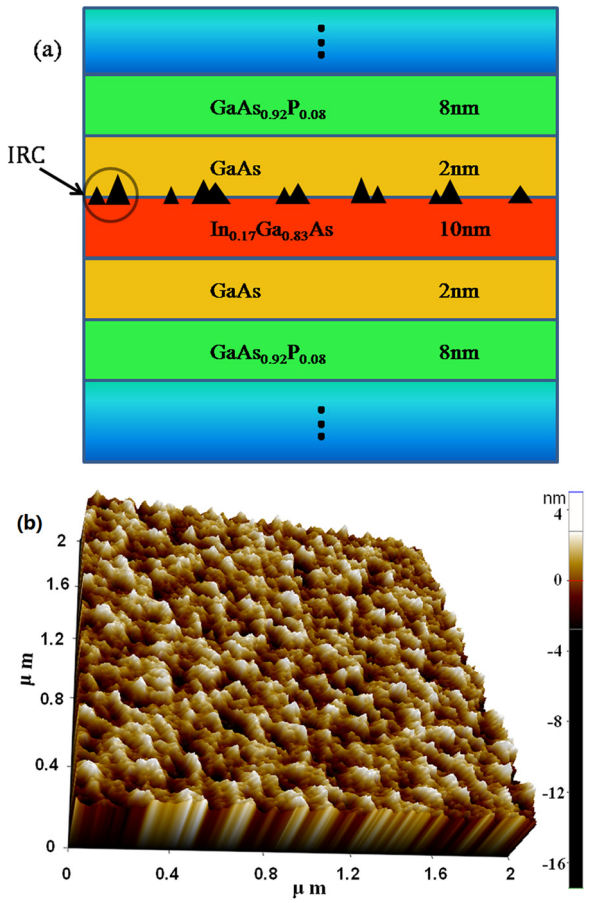

FIG. 1. (a) Layout of InGaAs-based IRC quantum-confined structure. (b) AFM image of IRCs on InGaAs surface.

recombination coefficients in the medium. The details of these coefficients can be obtained from Ref. 21 for InGaAs. Finally, A_p is the area of the optical injection, and N_w and L_w are the number and thickness, respectively, of the quantum-confined layers in the gain medium.

Figure 2(b) shows the results, where the dual peaks appear clearly in each APL spectrum. This phenomenon differs from the single-peak emission spectrum generated by a conventional quantum well and is attributed to all emissions from multiple $In_xGa_{1-x}As$ regions with varying indium content or band gaps and the presence of InAs clusters possible on the InGaAs surface due to IRCs. Based on bandgap and carrier-recombination calculations, the weaker peak at 930 nm corresponds exactly to emission from $In_xGa_{1-x}As$ with a fractional indium content $x = 0.12$. These results indicate that the IRCs remove indium from $In_{0.17}Ga_{0.83}As$, thereby forming multiple InGaAs regions, including at least $In_{0.17}Ga_{0.83}As$ and $In_{0.12}Ga_{0.88}As$.

We now discuss the contribution of IRCs to the APL spectrum. Based on the principle of the IRC formation and on published results,[17–19] the IRCs on the InGaAs surface may be composed of indium atoms, InAs clusters, or both. If IRCs contain only indium atoms, they would not contribute to the emission in 900–1000 nm range. However, if the clusters involve 20–200 nm InAs features, as

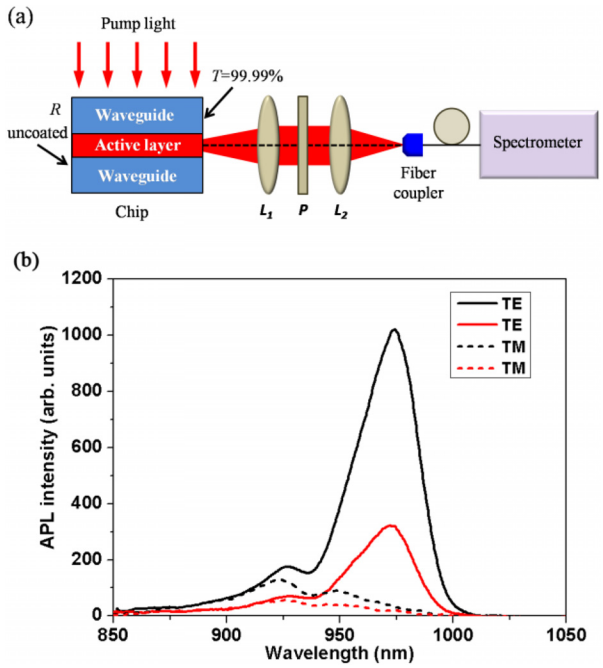

FIG. 2. (a) Schematic diagram of experimental setup for APL measurement from the facet of edge-emitting SOA sample. (b) APL spectra of TE and TM modes, measured with a carrier density of $4.8 \times 10^{17}\,\mathrm{cm}^{-3}$. The black and red curves show the APL intensity measured from the coated and uncoated ends, respectively.

stated above, they can be considered as InAs quantum dots. Such a scenario would allow IRCs to contribute to the emission spectrum in Fig. 2(b) because InAs/GaAs quantum dots can emit from 900 to 1500 nm, depending on their size. Further investigation is required to determine the detailed composition of IRCs and characterize their emission. In the present work, we focus on polarization-independent optical amplification by TE and TM gain.

The modal gain was determined by recording APL spectra from each end of the edge-emitting device and calculating the gain as follows:[22]

$$G = \frac{1}{L}\ln\frac{(1-R)I_{APL1} - I_{APL2}}{RI_{APL2}}, \tag{2}$$

where I_{APL1} and I_{APL2} are the measured APL intensities from the coated and uncoated ends of the sample, respectively, L is the single-pass distance traveled by light transmitted through the device, and R is the reflectivity of the InGaAs material, which was calculated to be approximately 30% based on the optical parameters of the material.

Figure 3(a) shows the measured gain. For the given injected-carrier densities, the TE- and TM-mode gain is comparable over a broad spectral range of roughly 65 nm, which offers the possibility of achieving optical amplification independent of polarization. The mechanism that produces these results differs from the mechanism at work in conventional quantum wells or quantum dots and is associated with a complex energy-band structure caused by the compressive and tensile strains within the active layer.

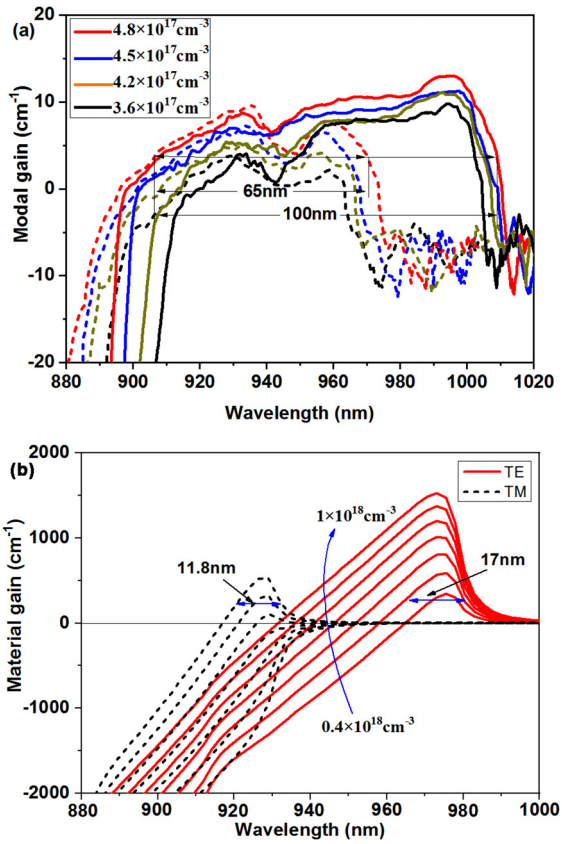

FIG. 3. (a) Measured modal gain from the sample for TE (solid curves) and TM (dashed curves) polarization modes. The injected-carrier density varies from 3.6 to $4.8 \times 10^{17}\,\mathrm{cm}^{-3}$. (b) Calculated material gain from a conventional 10-nm-thick $In_{0.17}Ga_{0.83}As/GaAs$ quantum well with no IRCs. The injected-carrier density varies from 0.4 to $1.0 \times 10^{18}\,\mathrm{cm}^{-3}$.

To compare with the gain characteristics of a conventional quantum well, we calculate the TE and TM gain of a conventional 10-nm-thick $In_{0.17}Ga_{0.83}As/GaAs$ compressively strained quantum well with a similar injected-carrier density. The result is shown in Fig. 3(b). Compared with the result shown in Fig. 3(a), the full width at half maximum of the gain from the IRC structure increases significantly for both TE and TM modes under a similar injected-carrier density of $4.8 \times 10^{17}\,\mathrm{cm}^{-3}$. This result means that the optical amplification may be achieved over a very broad spectral range, which is attributed to the superposition of emission from all InGaAs regions in the active layer with differing indium content and also to InAs clusters that form because of the IRC effect.

The mechanism leading to these results is analyzed based on transition matrix element theory,[23] according to which the TE gain in a conventional quantum-confined structure dominates the TM gain if the structure is subjected to compressive strain. In this case, carriers recombine mainly between the conduction band C_1 and the heavy-hole subband (HH_1) in the valence band. However, the TM gain becomes dominant if the structure is subjected to tensile strain, in which case carriers recombine mainly between the conduction band C_1 and the light-hole subband (LH_1) in the valence band.

To understand comparable TE and TM gain in a given sample, we use a step-well model (see Fig. 4), which is based on the dual peak in the APL spectra in Fig. 2(b). The peaks at 930 and 980 nm correspond to emission from $In_{0.12}Ga_{0.88}As$ and $In_{0.17}Ga_{0.83}As$, where $In_{0.12}Ga_{0.88}As$ forms due to the loss of indium atoms from the original $In_{0.17}Ga_{0.83}As$. The subsequent lattice mismatch produces tensile strain in $In_{0.12}Ga_{0.88}As$, whereas the lattice mismatch in $In_{0.17}Ga_{0.83}As$ leads to compressive strain. Thus, both compressive and tensile strain exists within the active layer, which forms the band structure shown in Fig. 4 in which the black and pink lines in the valence band denote the HH_1 and LH_1 bands, respectively. In this case, carriers recombine between the C_1 and HH_1 bands to produce TE emission and between the C_1 and LH_1 bands to produce TM emission. As a result, the device provides gain for both TE and TM polarization.

If the TE- and TM-polarized optical waves are of the same wavefield mode, which is typically the fundamental wave mode of the device, the confinement factor $\Gamma = \Gamma_x\Gamma_y\Gamma_z$ of the device is the same for the TE and TM wave fields. In this work, we obtain $\Gamma = 0.33\%$.[23] Optical amplification by a SOA can be described by

$$I_{\text{out}} = I_{\text{in}}e^{GL}, \tag{3}$$

where I_{in} (I_{out}) is the input (output) wave intensity of the SOA. Since many factors combine to determine the waveguide losses for the TE and TM wave fields (e.g., the optical gain, the material parameters, the geometry to couple light into the device, and the optical wave modes), determining the waveguide loss is complicated. To simply this problem, we consider only the fundamental wave mode for TE and TM polarization, in which case the waveguide losses are the same for TE and TM optical amplification and can be neglected in the analysis of polarization-independent optical amplification.

Figure 5 shows the results. Figure 5(a) shows the TE and TM optical amplification provided by the IRC device for several injected-carrier densities. These results are based on the gain data of Fig. 3(a) and Eq. (3). Figure 5(b) shows the intensity difference $\delta_{\text{TE-TM}}$ between the TE and TM optical amplification. The results show very little difference in intensity ($|\delta_{\text{TE-TM}}| < 0.5$ dB) over a spectral range of roughly 65 nm. These results show that the IRC quantum-confined

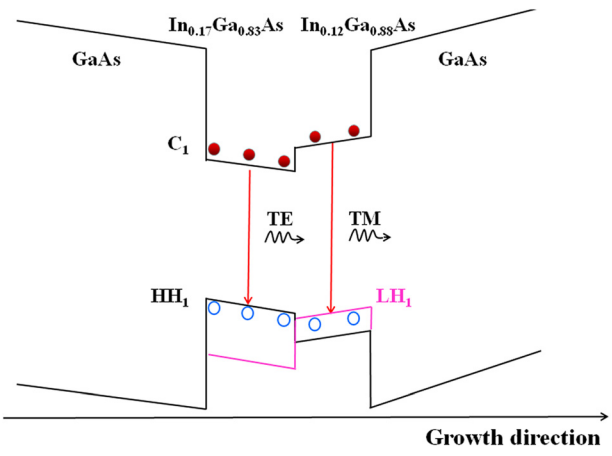

FIG. 4. Composite energy-band structure that forms because of IRC effect in InGaAs/GaAs.

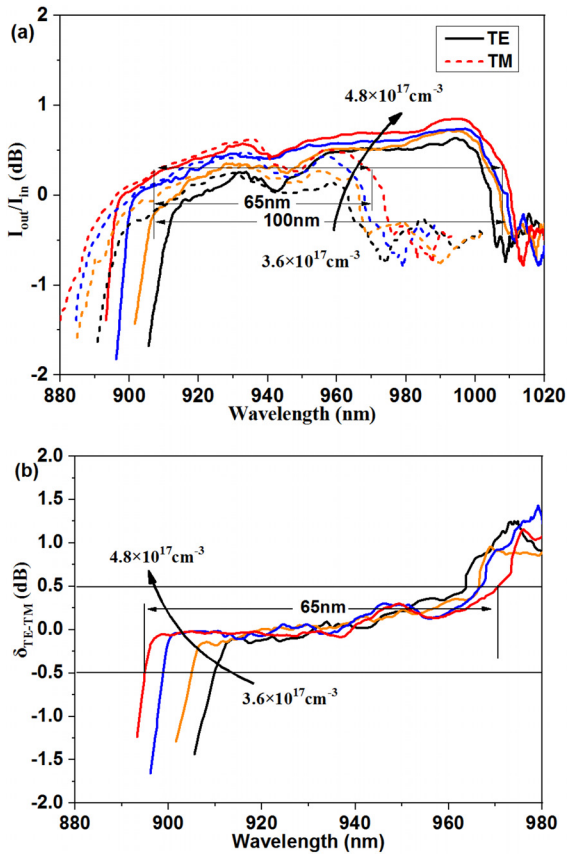

FIG. 5. (a) Relative intensity of TE and TM optical amplification through IRC structure with injected-carrier densities of 3.6–4.8 × 10^{17} cm^{-3} based on the gain data from Fig. 3(a). (b) Difference in intensity between TE and TM optical amplification with carrier density varying from 3.6 to 4.8 × $10^{17}$$cm^{-3}$.

device should provide equivalent optical amplification of TE and TM radiation over a broad spectral range of 65 nm.

These results were obtained in the 980 nm band of InGaAs-based materials. Given that InGaN produces a very broad emission spectrum from the visible to the C band, one may also expect similar results in the O and C bands of InGaN-based materials because IRCs may also form in these materials.[24–26]

In conclusion, we report the use of an InGaAs-based IRC quantum-confined structure as gain medium to realize polarization-independent optical amplification over an ultrabroad spectral range. The experimental results show that comparable optical gain is obtained simultaneously from both TE and TM polarization over a spectral range of 65 nm. This result opens the possibility of polarization-independent optical amplification over a broad spectral range. A preliminary analysis of the emission mechanism induced by the IRC structure indicates that the IRCs modify the original InGaAs active layer into numerous anisotropic InGaAs regions of varying indium, thereby producing hybrid strain states comprising both compressive and tensile strain in the active layer. This physical structure leads to a complex energy-band structure that allows the amplification of both TE and TM polarization and that we interpret via a step-well

model. We thus expect such IRC quantum-confined devices to offer comparable TE and TM optical amplification over a broad spectral range.

The authors gratefully acknowledge financial support from the National Natural Science Foundation of China (Grant Nos. 61874117 and 61474118) for this work.

DATA AVAILABILITY

The data that support the findings of this study are available from the corresponding author upon reasonable request.

REFERENCES

[1]T. Kamiya and M. Tsuchiya, Jpn. J. Appl. Phys., Part 1 **44**, 5875 (2005).
[2]J. M. Tang, P. S. Spencer, and K. A. Shore, Opt. Lett. **24**, 1605 (1999).
[3]Y. Jiang, C. Tang, and B. Yang, Electron. Lett. **45**, 303 (2009).
[4]G. Y. Chu, A. Maho, I. Cano, V. Polo, R. Brenot, H. Debrégeas, and J. Prat, Opt. Lett. **41**, 4696 (2016).
[5]H. X. Chen, Opt. Lett. **30**, 619 (2005).
[6]L. F. Tiemeijer, P. J. A. Thijs, T. van Dongen, R. W. M. Slootweg, J. M. M. van der Heijden, J. J. M. Binsma, and M. P. C. M. Krijn, Appl. Phys. Lett. **62**, 826 (1993).
[7]M. A. Newkirk, B. I. Miller, U. Koren, M. G. Young, M. Chien, R. M. Jopson, and C. A. Burrus, IEEE Photonics Technol. Lett. **5**, 406 (1993).
[8]J. E. M. Haverkort, B. H. P. Dorren, M. Kemerink, A. Y. Silov, and J. H. Wolter, Appl. Phys. Lett. **75**, 2782 (1999).
[9]R. Prasanth, J. E. M. Haverkort, and J. H. Wolter, Appl. Phys. Lett. **88**, 062108 (2006).
[10]K. Magari, M. Okamoto, Y. Suzuki, K. Sato, Y. Noguchi, and O. Mikami, IEEE J. Quantum Electron. **30**, 695 (1994).
[11]A. Ougazzaden, D. Sigogne, A. Mircea, E. V. K. Rao, A. Ramdane, and L. Silvestre, Electron. Lett. **31**, 1242 (1995).
[12]A. Godefroy, A. Le Corre, F. Clerot, S. Salaun, S. Loualiche, J. C. Simon, L. Henry, C. Vaudry, J. C. Keromnes, G. Joulie, and P. Lamouler, IEEE Photonics Technol. Lett. **7**, 473 (1995).
[13]J.-Y. Emery, P. Doussiere, L. Goldstein, F. Pommerceau, C. Fortin, R. Ngo, N. Tscherptner, J.-L. Lafragette, P. Auibert, and F. Brillouet, in *Proceedings 22 European Conference on Optical Communications (ECOC), Oslo Norway* (Telenor R&D, Kjeller, Norway), p. 3165.
[14]N. Yasuoka, K. Kawaguchi, H. Ebe, T. Akiyama, M. Ekawa, S. Tanaka, K. Morito, M. Sugawara, and Y. Arakawa, Appl. Phys. Lett. **92**, 101108 (2008).
[15]N. Yasuoka, K. Kawaguchi, H. Ebe, T. Akiyama, M. Ekawa, K. Morito, M. Sugawara, and Y. Arakawa, IEEE Photonics Technol. Lett. **20**, 1908 (2008).
[16]Q. Yu, M. Zheng, H. Tai, W. Lu, Y. Shi, J. Yue, X. Zhang, Y. Ning, and J. Wu, ACS Photonics **6**, 1990 (2019).
[17]A. Jasik, A. Wnuk, A. Wojcik-Jedlinska, R. Jakiela, J. Muszalski, W. Strupinski, and M. Bugajski, J. Cryst. Growth **310**, 2785 (2008).
[18]D. Schlenker, T. Miyamoto, Z. Chen, F. Koyama, and K. Iga, J. Cryst. Growth **209**, 27 (2000).
[19]H. P. Yu, C. Roberts, and R. Murray, Appl. Phys. Lett. **66**, 2253 (1995).
[20]K. Muraki, S. Fukatsu, Y. Shiraki, and R. Ito, Appl. Phys. Lett. **61**, 557 (1992).
[21]M. Kuznetsov, F. Hakimi, R. Sprague, and A. Mooradian, IEEE J. Sel. Top. Quantum Electron. **5**, 561 (1999).
[22]M. L. Ma, J. Wu, Y. Q. Ning, F. Zhou, M. Yang, X. Zhang, J. Zhang, and G. Y. Shang, Opt. Express **21**, 10335 (2013).
[23]L. A. Coldren and S. W. Corzine, *Diode Lasers and Photonic Integrated Circuits*, 2nd ed. (Wiley, New York, 2012).
[24]W.-C. Tsai, H. Lin, W.-C. Ke, W.-H. Chang, W.-C. Chou, W.-K. Chen, and M.-C. Lee, Phys. Status Solidi C **5**, 1702 (2008).
[25]T.-J. Yang, R. Shivaraman, J. S. Speck, and Y.-R. Wu, J. Appl. Phys. **116**, 113104 (2014).
[26]Y. Meng, L. Wang, G. Zhao, F. Li, H. Li, S. Yang, and Z. Wang, Phys. Status Solidi A **215**, 1800455 (2018).